ACS SENSORS

Letter

pubs.acs.org/acssensors

Identification of Nanoparticles with a Colorimetric Sensor Array

Morteza Mahmoudi,*[,†,‡] Samuel E. Lohse,[†] Catherine J. Murphy,[†] and Kenneth S. Suslick*[,†]

[†]Department of Chemistry, University of Illinois at Urbana−Champaign, 600 South Mathews Avenue, Urbana, Illinois 61801, United States

[‡]Department of Nanotechnology, Faculty of Pharmacy, Tehran University of Medical Sciences, Tehran, Iran

Supporting Information

ABSTRACT: A simple colorimetric sensor array technique was developed for the detection of various different nanoparticles (NPs) in aqueous solutions. The sensor array consists of five different cross-reactive chemoresponsive dyes, whose visible absorbances change in response to their interactions with NPs. Although no single dye is specific for any one NP, the pattern of color changes for all dyes provides a unique molecular fingerprint for each type of NP studied. Based on the responses of various dyes, a semiquantitative determination of concentration of each type of NP could also be accomplished with excellent sensitivity (<100 ng/mL). A variety of chemically distinct NPs were unambiguously identified using a standard chemometric approaches, including gold nanospheres (2 through 40 nm diameter), gold nanorods (2.4 and 3.5 aspect ratios), and multifunctional carbon nanospheres without errors in 112 trials. This colorimetric approach may pave the way for a fast, reliable, and inexpensive method to detect nanopollution and to characterize the physiochemical properties of NPs.

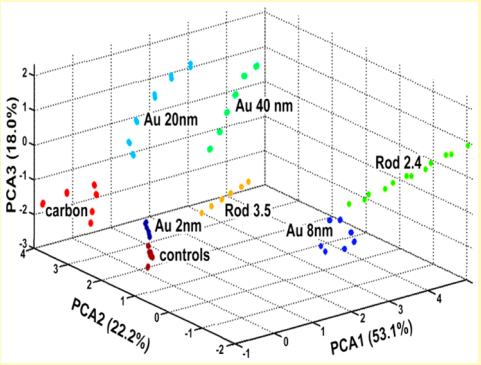

KEYWORDS: *sensor array, nanoparticles, gold nanorods, colorimetric*

Engineered nanoparticles (NPs) have now become prevalent in a variety of technology markets, including composites, coatings, electronics, information technology, healthcare, and biomedicine.[1−12] Due to the increasing prevalence of nanomaterials and nanomaterial-enabled products, human exposure to the NPs is now a prominent health and environmental concern.[13−16] There is a pressing need, then, for sensors that provide rapid, sensitive, and highly portable detection and identification of NPs, but detection of NPs in the environment has received relatively little study.[13,17,18] Ideally, such sensors should also be able to unambiguously discriminate among NPs with different sizes, shapes, core materials, and surface chemistries, especially since their physicochemical properties (e.g., chemical,[19] electrical,[20] optical,[21] magnetic,[22] and surface corona[11,22−25]) have substantial influence on their potential toxicity and environmental impact.

The use of optical sensors,[26−30] and especially the colorimetric sensor array,[26,31−33] has proven to be a fast, sensitive, and versatile method of liquid, vapor, and gas analysis where the specificity derives from the pattern of response from cross-reactive sensor arrays rather than individual sensors for specific analytes. Colorimetric sensor arrays have been successfully used to differentiate among diverse families of analytes, ranging from toxic industrial chemicals,[34−36] to explosives,[37−40] to various foods and beverages,[41−46] to pathogenic bacteria and fungi.[47−52] Here, we present the first example of a colorimetric array approach for the rapid and sensitive identification of a wide range of NPs in aqueous media.

Five water-soluble chemoresponsive dyes (specifically bromocresol green (BCG), bromophenol blue (BPB), bromophenol red (BPR), bromopyrogallol red (BGR), and acridine orange base (APB), as shown in Figure 1) were employed for detection and identification of NPs. We examined

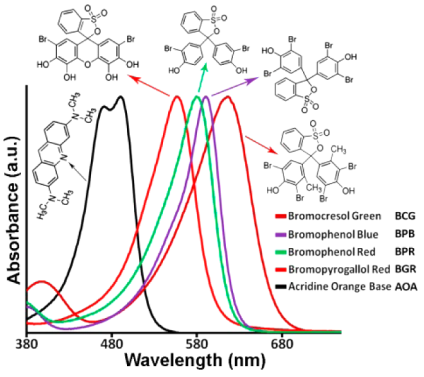

Figure 1. Structures, absorbance spectra, and abbreviations of the five dyes used in the colorimetric sensor array at pH of 7.4.

Received: August 7, 2015
Revised: October 21, 2015
Accepted: November 3, 2015
Published: November 3, 2015

DOI: 10.1021/acssensors.5b00014
ACS Sens. 2016, 1, 17−21

a representative set of seven nanoparticles and three controls: specifically, spherical gold nanoparticles in four different sizes, gold nanorods with two different aspect ratios, and a multifunctional carbon/iron oxide. Full details on the preparation and characterization of the employed NPs are presented in the Supporting Information (SI p. S1, Table S1, and Figures S1–S3). The Au NPs were positively charged (i.e., cetyltrimethylammonium bromide, CTAB-stablized, or poly-allylamine hydrochloride coated for 2 nm Au NPs only) with spherical (diameters of 2, 8, 20, and 40 nm) and rod (aspect ratios of 2.4 and 3.5) shapes, as well as multifunctional carbon-based (porous carbon spheres impregnated with magnetite NPs) particles. The selection of these NPs was based in part on their extensive usage in biomedical applications.[2,11,17,53,54]

The colorimetric sensor array approach has generally used printed dye arrays on porous membranes.[24,29−34] For application to the identification of nanoparticles, however, we made use of an array of solution phase sensors and generated color difference maps using changes in the visible absorbance spectra of the dyes in aqueous solutions before and after exposure to the NPs. In order to ensure reliable measurements of the color differences of the dyes before and after interaction with NPs, all measurements were performed under tight control of pH at 7.41 using standard phosphate buffered saline (PBS) solutions. Solutions of various dyes at various low concentrations of various NPs (ranging from 100 ng/mL to 1000 ng/mL with pH of 7.41) were prepared and their visible spectra were collected and analyzed (Figure 2 and Figures S4–S6). As seen in Figure 2, the color differences are often observable by eye.

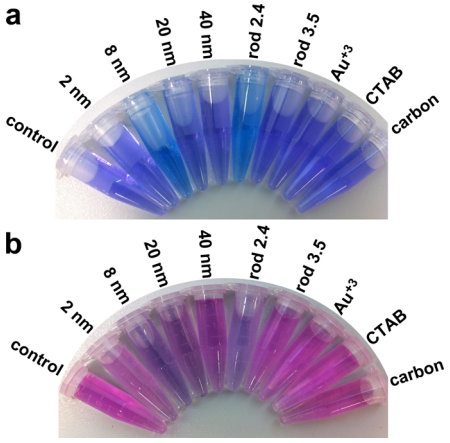

Figure 2. Color changes of dyes in aqueous solutions after interaction with NPs are visible even to the naked eye. Photographs of (a) BPB and (b) BGR solutions exposed to various NPs and controls (phosphate buffer, pH 7.4, Au^{3+} ions or CTAB surfactant) at concentration of 1 μg/mL. Solutions and spectra of all five dyes are provided in SI Figures S4–6. All solutions are in standard PBS solutions at pH 7.41.

Color-difference maps for the dyes were generated by subtraction of the light absorbance before exposure from that after exposure to NPs at 3 selected wavelengths (i.e., 480, 590, and 620 nm); these wavelengths represent near optimal choices for maximum color changes of the dye spectra (Figure 1). As seen in Figure 3, the difference maps of various dyes to the NPs provide unique fingerprint patterns that effectively identify the NPs and the concentration of each NP: even by eye, before statistical analysis, the array response to each NP is represented

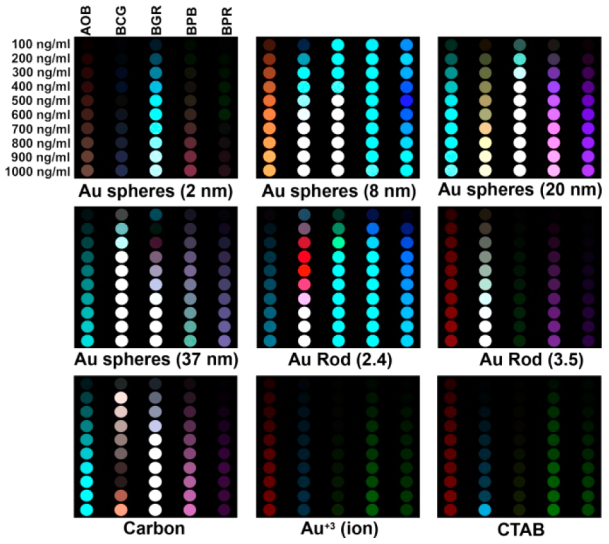

Figure 3. Color-change profiles of the five sensor dyes after interaction with various NPs at different NP concentrations. For display purposes, these difference maps were generated by subtraction of the solution absorbance before exposure from that after exposure to various NPs and controls (i.e., gold ions (Au^{3+}) and surfactant (CTAB)) with three selected wavelengths (i.e., 480, 590, and 620 nm) assigned to RGB values; at each of these three wavelengths, absorbances from 0 to 0.484 optical density were mapped linearly to 0 to 255 in RGB values.

by an identifiable pattern. Figure S7 presents the same patterns at specific concentrations for each nanoparticle.

Prior to sensing trials, the nanoparticle samples were extensively purified by either centrifugation or diafiltration (depending on AuNP size) in order to reduce free ligand, gold salt, and any gold nanoparticle byproducts to below detectable levels (i.e., less than ppm). It is worth noting that these possible interferents induce negligible response in the sensor in control experiments. For instance, doping phosphate buffered aqueous dye solutions with gold ions (100 to 1000 ng/mL of $HAuCl_4$) or with CTAB surfactant (100 to 1000 ng/mL) were evaluated as controls at comparable concentrations to the AuNP samples, but these control samples induced very limited responses in the sensor array and were clearly distinct from the NP samples. In addition, the spectra of the dyes with intentional small pH variations (i.e., pH 7.36 to 7.46, which is well outside of our measured variation in pH from solution to solution) were also examined; these small variations in pH had detectable effect on the absorbance spectra (see Figure S5). The origins of the observed color changes are therefore *not* due to changes in bulk pH or to interactions of the dyes with gold cations or surfactant anions. Instead, the color changes must reflect the local environment of the dyes associated with the interface of the nanoparticles: these interactions may include local pH effects, Lewis acid–base interactions, hydrogen bonding, and local polarity (solvatochromic effects).[26] The nature of the interfacial region of nanoparticles is a reflection of the physicochemical properties of each type of nanoparticle and therefore provides a means of nanoparticle identification.

The temporal behavior of the dye absorbance was also examined. Variations of the absorbance spectra after exposure to the different NPs taken a 1 min intervals up to 10 min are provided in Figure S6. The very large majority of the color changes occur in only a few seconds. In most cases, complete equilibration occurs within 1 or 2 min and rarely more than 3

DOI: 10.1021/acssensors.5b00014
ACS Sens. 2016, 1, 17−21

min. The slight delay in response is probably due to the exchange rate of the dyes into the "hard corona" (i.e., the more strongly adsorbed ions, molecules, and macromolecules associated with nanoparticles[11,22−25]).

The ability of this colorimetric approach to discriminate among even closely similar NPs at various concentrations is impressive. A principal component analysis (PCA) was completed on the digital color differences at 480, 590, and 620 nm. The eigenvectors generated by PCA defines the linear combinations of the response of each sensor (i.e., change in absorbance at each wavelength for each dye) that minimize the total variance into as few dimensions as possible.[55,56] The scree plot of the PCA (Figure S8) show that four dimensions are necessary to capture 95% of the total variance (and 7 dimensions for 99%). A three-dimensional score plot (Figure 4 and Figure S9) shows excellent resolution of the NPs from

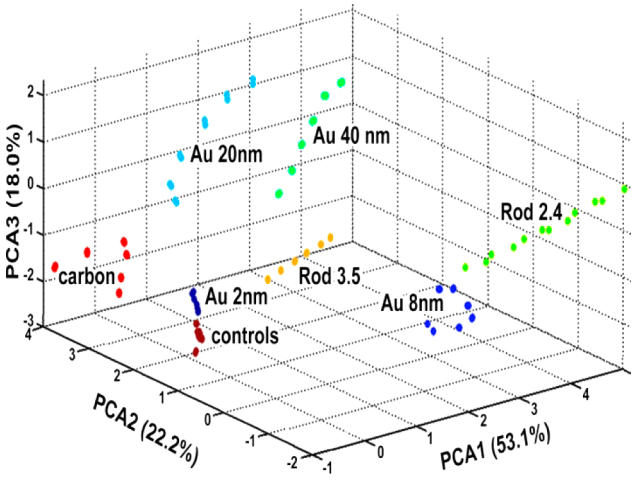

Figure 4. PCA score plot for various NPs at different concentrations and controls; the three dimensions shown capture 93.3% of the total variance, based on all 112 trials of seven types of NPs (with concentrations of 500, 600, 700, 800, 900, and 1000 ng/mL, duplicate trials) and controls (i.e., Au^{3+} ions, CTAB, and pH 7.36 to 7.46).

each other and from the controls. The trails of the points for each analyte represent the effect of NP concentration over the range plotted. At sufficiently low concentrations (well below 100 ng/mL), these trails will converge on the control (Figure S9): the concentrations at which a low concentration of a NP cannot be separated from the other NPs defines the limit of recognition, and the concentration at which any one NP can no longer be differentiated from the controls represents the limit of detection.

To further probe the ability of our colorimetric sensor array to discriminate among the types of nanoparticles, a hierarchical cluster analysis (HCA) was also done. HCA (unlike model-dependent analyses such as linear discriminant analysis or support vector machine analysis) is a model-free statistical approach that makes no a priori assumptions about the class identification of data.[55,56] The resulting dendrogram is shown in Figure 5; each of the 7 types of nanoparticle was represented by 12 individual trials ranging in concentration from 500 to 1000 ng/mL with an additional 28 control trials (i.e., Au ions, CTAB, and pH 7.36 to 7.46)) for a total n = 112. The HCA dendrogram shows perfect discrimination without misclassification or confusion among all the types of nanoparticles (i.e., error rate <0.9%).

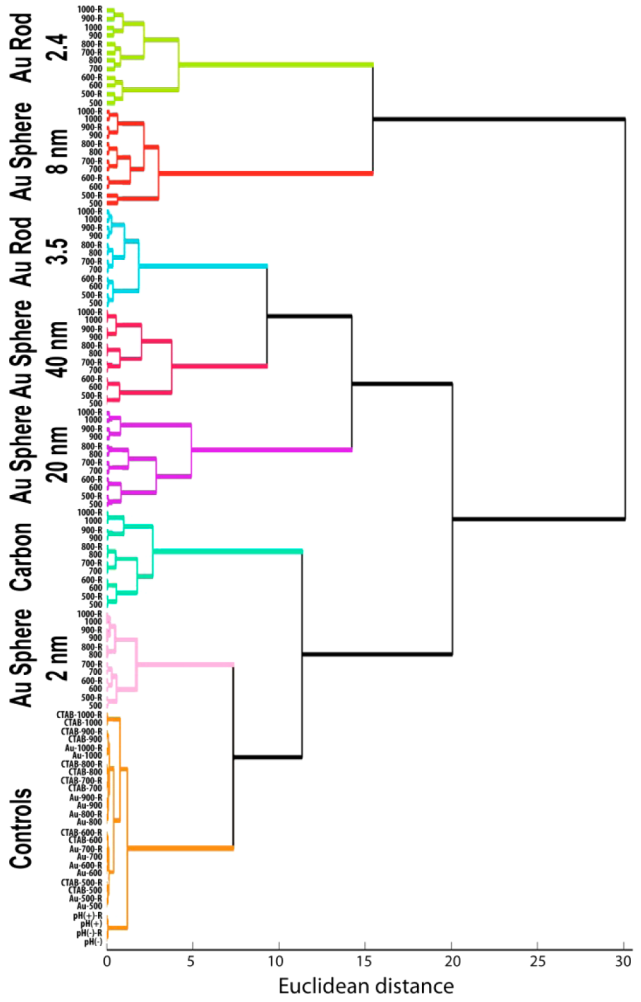

Figure 5. Dendrogram generated by hierarchical cluster analysis (HCA) of the color changes of the sensor dyes upon exposure to various NPs at different concentrations and controls (i.e., Au ions, CTAB, and pH varied from 7.36 to 7.46). Analyte labels indicate NP identity and concentration; all experiments were run in duplicate (-R corresponds to the replicates): no confusion or errors in classification were observed among the 112 trials. Clustering in the HCA used minimum variance (Ward's Method[56]).

In summary, we have demonstrated a simple colorimetric sensor array approach capable of detection and unambiguous differentiation of a wide range of NPs. The sensor array is able to discriminate among different sizes, shapes, and compositions of NPs over a range of concentrations with extremely high accuracy. This approach may prove useful for the rapid identification of nanopollutants (for example, even in the field after microfiltration and buffering of samples) and may also be a useful probe of the protein corona identity of nanoparticles (which remains a major current challenge in nanobiointerfaces).

■ ASSOCIATED CONTENT

Supporting Information

The Supporting Information is available free of charge on the ACS Publications website at DOI: 10.1021/acssensors.5b00014.

Full experimental details, characterization of the nanoparticles, and PCA graphs (PDF)

DOI: 10.1021/acssensors.5b00014
ACS Sens. 2016, 1, 17−21

AUTHOR INFORMATION

Corresponding Authors

*E-mail: mahmoudi-m@tums.ac.ir.

*E-mail: ksuslick@illinois.edu.

Notes

The authors declare no competing financial interest.

ACKNOWLEDGMENTS

This work was supported by the U.S. NSF (CHE-1152232).

REFERENCES

(1) Schmid, G. *Nanoparticles: From Theory to Application*. 2nd ed.; Wiley-VCH: Weinheim, 2010.

(2) Alkilany, A. M.; Lohse, S. E.; Murphy, C. J. The Gold Standard: Gold Nanoparticle Libraries To Understand the Nano-Bio Interface. *Acc. Chem. Res.* **2013**, *46*, 650−661.

(3) Li, N.; Zhao, P.; Astruc, D. Anisotropic Gold Nanoparticles: Synthesis, Properties, Applications, and Toxicity. *Angew. Chem., Int. Ed.* **2014**, *53*, 1756−1789.

(4) Zeng, S.; Baillargeat, D.; Ho, H.-P.; Yong, K.-T. Nanomaterials enhanced surface plasmon resonance for biological and chemical sensing applications. *Chem. Soc. Rev.* **2014**, *43*, 3426−3452.

(5) Bartelmess, J.; Quinn, S. J.; Giordani, S. Carbon nanomaterials: multi-functional agents for biomedical fluorescence and Raman imaging. *Chem. Soc. Rev.* **2015**, *44*, 4672−4698.

(6) Lim, E.-K.; Kim, T.; Paik, S.; Haam, S.; Huh, Y.-M.; Lee, K. Nanomaterials for Theranostics: Recent Advances and Future Challenges. *Chem. Rev.* **2015**, *115*, 327−394.

(7) Zhang, D. Y.; Seelig, G. Dynamic DNA nanotechnology using strand-displacement reactions. *Nat. Chem.* **2011**, *3*, 103−113.

(8) Astruc, D. Electron-transfer processes in dendrimers and their implication in biology, catalysis, sensing and nanotechnology. *Nat. Chem.* **2012**, *4*, 255−267.

(9) Linic, S.; Christopher, P.; Ingram, D. B. Plasmonic-metal nanostructures for efficient conversion of solar to chemical energy. *Nat. Mater.* **2011**, *10*, 911−921.

(10) Mahmoudi, M.; Abdelmonem, A. M.; Behzadi, S.; Clement, J. H.; Dutz, S.; Ejtehadi, M. R.; Hartmann, R.; Kantner, K.; Linne, U.; Maffre, P. Temperature: The "Ignored" Factor at the NanoBio Interface. *ACS Nano* **2013**, *7*, 6555−6562.

(11) Mahmoudi, M.; Lohse, S. E.; Murphy, C. J.; Fathizadeh, A.; Montazeri, A.; Suslick, K. S. Variation of Protein Corona Composition of Gold Nanoparticles Following Plasmonic Heating. *Nano Lett.* **2014**, *14*, 6−12.

(12) Bang, J. H.; Suslick, K. S. Applications of Ultrasound to the Synthesis of Nanostructured Materials. *Adv. Mater.* **2010**, *22*, 1039−1059.

(13) Peijnenburg, W. J. G. M.; Baalousha, M.; Chen, J.; Chaudry, Q.; Von der kammer, F.; Kuhlbusch, T. A. J.; Lead, J.; Nickel, C.; Quik, J. T. K.; Renker, M.; Wang, Z.; Koelmans, A. A. A Review of the Properties and Processes Determining the Fate of Engineered Nanomaterials in the Aquatic Environment. *Crit. Rev. Environ. Sci. Technol.* **2015**, *45*, 2084−2134.

(14) Wagner, S.; Gondikas, A.; Neubauer, E.; Hofmann, T.; von der Kammer, F. Spot the Difference: Engineered and Natural Nanoparticles in the Environment-Release, Behavior, and Fate. *Angew. Chem., Int. Ed.* **2014**, *53*, 12398−12419.

(15) Mahmoudi, M.; Hofmann, H.; Rothen-Rutishauser, B.; Petri-Fink, A. Assessing the In Vitro and In Vivo Toxicity of Superparamagnetic Iron Oxide Nanoparticles. *Chem. Rev.* **2012**, *112*, 2323−2338.

(16) Ghafariyan, M. H.; Malakouti, M. J.; Dadpour, M. R.; Stroeve, P.; Mahmoudi, M. Effects of Magnetite Nanoparticles on Soybean Chlorophyll. *Environ. Sci. Technol.* **2013**, *47*, 10645−10652.

(17) Alkilany, A. M.; Murphy, C. J. Toxicity and cellular uptake of gold nanoparticles: what we have learned so far? *J. Nanopart. Res.* **2010**, *12*, 2313−2333.

(18) Maurer-Jones, M. A.; Gunsolus, I. L.; Murphy, C. J.; Haynes, C. L. Toxicity of Engineered Nanoparticles in the Environment. *Anal. Chem.* **2013**, *85*, 3036−3049.

(19) El-Sayed, M. A. Some interesting properties of metals confined in time and nanometer space of different shapes. *Acc. Chem. Res.* **2001**, *34*, 257−264.

(20) Daniel, M. C.; Astruc, D. Gold Nanoparticles: Assembly, Supramolecular Chemistry, Quantum-Size-Related Properties, and Applications Toward Biology, Catalysis, and Nanotechnology. *Chem. Rev.* **2004**, *104*, 293−346.

(21) de la Rica, R.; Stevens, M. M. Plasmonic ELISA for the ultrasensitive detection of disease biomarkers with the naked eye. *Nat. Nanotechnol.* **2012**, *7*, 821−824.

(22) Mahmoudi, M.; Lynch, I.; Ejtehadi, M. R.; Monopoli, M. P.; Bombelli, F. B.; Laurent, S. Protein−Nanoparticle Interactions: Opportunities and Challenges. *Chem. Rev.* **2011**, *111*, 5610−5637.

(23) Cedervall, T.; Lynch, I.; Lindman, S.; Berggård, T.; Thulin, E.; Nilsson, H.; Dawson, K. A.; Linse, S. Understanding the nanoparticle−protein corona using methods to quantify exchange rates and affinities of proteins for nanoparticles. *Proc. Natl. Acad. Sci. U. S. A.* **2007**, *104*, 2050−2055.

(24) Monopoli, M. P.; Bombelli, F. B.; Dawson, K. A. Nanobiotechnology: Nanoparticle coronas take shape. *Nat. Nanotechnol.* **2011**, *6*, 11−12.

(25) Kelly, P. M.; Åberg, C.; Polo, E.; O'Connell, A.; Cookman, J.; Fallon, J.; Krpetić, Ž.; Dawson, K. A. Mapping protein binding sites on the biomolecular corona of nanoparticles. *Nat. Nanotechnol.* **2015**, *10*, 472−479.

(26) Askim, J. R.; Mahmoudi, M.; Suslick, K. S. Optical sensor arrays for chemical sensing: the optoelectronic nose. *Chem. Soc. Rev.* **2013**, *42*, 8649−8682.

(27) McDonagh, C.; Burke, C. S.; MacCraith, B. D. Optical Chemical Sensors. *Chem. Rev.* **2008**, *108*, 400−422.

(28) Stewart, S.; Ivy, M. A.; Anslyn, E. V. The use of principal component analysis and discriminant analysis in differential sensing routines. *Chem. Soc. Rev.* **2014**, *43*, 70−84.

(29) Diehl, K. L.; Anslyn, E. V. Array sensing using optical methods for detection of chemical and biological hazards. *Chem. Soc. Rev.* **2013**, *42*, 8596−8611.

(30) Lu, Y. X. Optical Chemical Sensor Array Based on Functional Nanomaterials. *Progress in Chemistry* **2014**, *26*, 931−938.

(31) Janzen, M. C.; Ponder, J. B.; Bailey, D. P.; Ingison, C. K.; Suslick, K. S. Colorimetric sensor Arrays for volatile organic compounds. *Anal. Chem.* **2006**, *78*, 3591−3600.

(32) Rakow, N. A.; Suslick, K. S. A colorimetric sensor array for odour visualization. *Nature* **2000**, *406*, 710−713.

(33) Askim, J. R.; Suslick, K. S. Hand-Held Reader for Colorimetric Sensor Arrays. *Anal. Chem.* **2015**, *87*, 7810−7816.

(34) Lim, S. H.; Feng, L.; Kemling, J. W.; Musto, C. J.; Suslick, K. S. An optoelectronic nose for the detection of toxic gases. *Nat. Chem.* **2009**, *1*, 562−567.

(35) Feng, L.; Musto, C. J.; Kemling, J. W.; Lim, S. H.; Suslick, K. S. A colorimetric sensor array for identification of toxic gases below permissible exposure limits. *Chem. Commun.* **2010**, *46*, 2037−2039.

(36) Feng, L.; Musto, C. J.; Kemling, J. W.; Lim, S. H.; Zhong, W.; Suslick, K. S. Colorimetric sensor array for determination and identification of toxic industrial chemicals. *Anal. Chem.* **2010**, *82*, 9433−9440.

(37) Lin, H.; Suslick, K. S. A colorimetric sensor array for detection of triacetone triperoxide vapor. *J. Am. Chem. Soc.* **2010**, *132*, 15519−15521.

(38) Li, Z.; Bassett, W. P.; Askim, J. R.; Suslick, K. S. Differentiation among peroxide explosives with an optoelectronic nose. *Chem. Commun.* **2015**, *51*, 15312−15315.

(39) Li, Z.; Jang, M.; Askim, J. R.; Suslick, K. S. Identification of accelerants, fuels and post-combustion residues using a colorimetric sensor array. *Analyst* **2015**, *140*, 5929−5935.

DOI: 10.1021/acssensors.5b00014
ACS Sens. 2016, 1, 17−21

(40) Askim, J. R.; Li, Z.; LaGasse, M. K.; Rankin, J. M.; Suslick, K. S. An optoelectronic nose for identification of explosives. *Chem. Sci.* **2015**, in press. DOI: 10.1039/C5SC02632F.
(41) Zhang, C.; Bailey, D. P.; Suslick, K. S. Colorimetric sensor arrays for the analysis of beers: A feasibility study. *J. Agric. Food Chem.* **2006**, *54*, 4925−4931.
(42) Zhang, C.; Suslick, K. S. Colorimetric sensor array for soft drink analysis. *J. Agric. Food Chem.* **2007**, *55*, 237−242.
(43) Suslick, B. A.; Feng, L.; Suslick, K. S. Discrimination of complex mixtures by a colorimetric sensor array: Coffee aromas. *Anal. Chem.* **2010**, *82*, 2067−2073.
(44) Huang, X. W.; Zou, X. B.; Shi, J. Y.; Guo, Y. N.; Zhao, J. W.; Zhang, J. C.; Hao, L. M. Determination of pork spoilage by colorimetric gas sensor array based on natural pigments. *Food Chem.* **2014**, *145*, 549−554.
(45) Li, J. J.; Song, C. X.; Hou, C. J.; Huo, D. Q.; Shen, C. H.; Luo, X. G.; Yang, M.; Fa, H. B. Development of a Colorimetric Sensor Array for the Discrimination of Chinese Liquors Based on Selected Volatile Markers Determined by GC-MS. *J. Agric. Food Chem.* **2014**, *62*, 10422−10430.
(46) Zaragoza, P.; Ros-Lis, J. V.; Vivancos, J. L.; Martinez-Manez, R. Proof of concept of using chromogenic arrays as a tool to identify blue cheese varieties. *Food Chem.* **2015**, *172*, 823−830.
(47) Carey, J. R.; Suslick, K. S.; Hulkower, K. I.; Imlay, J. A.; Imlay, K. R. C.; Ingison, C. K.; Ponder, J. B.; Sen, A.; Wittrig, A. E. Rapid identification of bacteria with a disposable colorimetric sensing array. *J. Am. Chem. Soc.* **2011**, *133*, 7571−7576.
(48) Shetty, V.; Zigler, C.; Robles, T. F.; Elashoff, D.; Yamaguchi, M. Developmental validation of a point-of-care, salivary alpha-amylase biosensor. *Psychoneuroendocrinology* **2011**, *36*, 193−199.
(49) Lonsdale, C. L.; Taba, B.; Queralto, N.; Lukaszewski, R. A.; Martino, R. A.; Rhodes, P. A.; Lim, S. H. The Use of Colorimetric Sensor Arrays to Discriminate between Pathogenic Bacteria. *PLoS One* **2013**, *8*, e62726.
(50) Chen, Q. S.; Li, H. H.; Ouyang, Q.; Zhao, J. W. Identification of spoilage bacteria using a simple colorimetric sensor array. *Sens. Actuators, B* **2014**, *205*, 1−8.
(51) Zaragoza, P.; Fernandez-Segovia, I.; Fuentes, A.; Vivancos, J. L.; Ros-Lis, J. V.; Barat, J. M.; Martinez-Manez, R. Monitorization of Atlantic salmon (Salmo salar) spoilage using an optoelectronic nose. *Sens. Actuators, B* **2014**, *195*, 478−485.
(52) Zhang, Y.; Askim, J. R.; Zhong, W.; Orlean, P.; Suslick, K. S. Identification of pathogenic fungi with an optoelectronic nose. *Analyst* **2014**, *139*, 1922−1928.
(53) Mahmoudi, M.; Serpooshan, V.; Laurent, S. Engineered nanoparticles for biomolecular imaging. *Nanoscale* **2011**, *3*, 3007−3026.
(54) Atkinson, J. D.; Fortunato, M. E.; Dastgheib, S. A.; Rostam-Abadi, M.; Rood, M. J.; Suslick, K. S. Synthesis and characterization of iron-impregnated porous carbon spheres prepared by ultrasonic spray pyrolysis. *Carbon* **2011**, *49*, 587−598.
(55) Janata, J. *Principles of Chemical Sensors*, 2nd ed.; Springer: New York, 2009.
(56) Johnson, R. A.; Wichern, D. W. *Applied Multivariate Statistical Analysis*, 6th ed.; Prentice Hall: New York, 2007.

DOI: 10.1021/acssensors.5b00014
ACS Sens. 2016, 1, 17−21